Finite-temperature properties of the triangular lattice *t-J* model and applications to Na_xCoO_2

Jan O. Haerter, Michael R. Peterson, and B. Sriram Shastry
Physics Department, University of California, Santa Cruz, California 95064, USA
(Received 31 July 2006; revised manuscript received 9 October 2006; published 22 December 2006)

We present a finite temperature (T) study of the *t-J* model on the two-dimensional triangular lattice for the negative hopping t, as relevant for the electron-doped Na_xCoO_2 (NCO). We study several thermodynamic and transport properties in this study: the T-dependent chemical potential, specific heat, magnetic susceptibility, and the dynamic Hall coefficient across the entire doping range. We show systematically how this simplest model for strongly correlated electrons describes a crossover as function of doping (x) from a Pauli-like weakly spin-correlated metal close to the band limit (density $n=2$) to the Curie-Weiss metallic phase ($1.5<n<1.75$) with pronounced antiferromagnetic (AFM) correlations at low temperatures and Curie-Weiss-type behavior in the high-temperature regime. Upon further reduction of the doping, a different energy scale, dominated by spin-interactions (J) emerges. It is apparent both in specific heat and susceptibility, and we identify an effective interaction $J_{eff}(x)$, valid across the entire doping range. This is in contrast to the formula by Anderson *et al.* [J. Phys.: Condens. Matter **16**, R755 (2004)] for the square lattice. NCO has $t<0$, hence the opposite sign of the Nagaoka-ferromagnetic situation, this expression includes the subtle effect of weak kinetic AFM [Haerter and Shastry, Phys. Rev. Lett. **95**, 087202 (2005)], as encountered in the infinitely correlated situation ($U=\infty$) for electronic frustration. By explicit computation of the Kubo formulas, we address the question of practical relevance of the high-frequency expression for the Hall coefficient R_H^* [Shastry *et al.*, Phys. Rev. Lett. **70**, 2004 (1993)]. We hope to clarify some open questions concerning the applicability of the *t-J* model to real experimental situations through this study.

DOI: 10.1103/PhysRevB.74.245118 PACS number(s): 72.15.Jf, 65.90.+i, 71.27.+a

I. INTRODUCTION

Since the discovery of superconductivity for $x\sim 0.3$ in H_2O-intercalated Na_xCoO_2, or NCO crystals,[4] this compound has drawn significant attention. NCO also displays a variety of remarkable thermoelectric effects, such as an unusually large and magnetic-field dependent thermopower[5] for $x\sim 0.66$ and a T-linear Hall coefficient.[3,6] While some of its properties are similar to those seen in high-T_c materials there are some major differences. Both the cobaltates and the cuprates become superconducting in the vicinity of half filling. However, in NCO this is enabled through electron doping x between $x=1/4$ and $x=1/3$,[7] while the cuprates require hole doping. For both compounds the role of electron transport in two-dimensional planes—separated by thick insulating layers—appears to be crucial. While the cuprates have planar square lattices (Cu ions), a triangular lattice (Co atoms) results in NCO. The magnitude of the hopping integral seems to be an order of magnitude smaller in NCO (Ref. 8) than in the cuprates, thus leading to a lower temperature scale for all physical phenomena. The experimental results indicate a rich set of phases with x, and it seems difficult to obtain these from a single simple model. However, the fundamental model of strong correlations, namely the *t-J* model, seems very promising in terms of explaining transport and thermodynamic phenomena, and that is precisely the aim of this paper.

In the half filled band, where strong interactions lead to the spin-$\frac{1}{2}$ Heisenberg antiferromagnet (HAF), the square geometry facilitates antiferromagnetism through its bipartite nature, while the tendency towards antiferromagnetism in the cobaltate system is weaker. However, extensive numerical computations[9] indicate Néel long-ranged order even in the triangular lattice. Away from half filling, projected hopping on the hole-doped ($n<1$) square lattice system ($t<0$) obeys the Nagaoka mechanism.[10] This results in a competition between the ferromagnetic (FM) kinetic operator and antiferromagnetic (AFM) potential energy for finite values of J leading to the formula espoused by Anderson *et al.*, $J_{eff}\sim J-4x|t|$. Conversely, in the current case of the electron-doped triangular lattice ($n>1$) with a negative hopping $t<0$, AFM tendencies are *enhanced* by the electronically frustrated kinetic energy operator, a phenomenon that we have previously named *kinetic antiferromagnetism* (KA) in the case of a single hole in the infinite U limit.[2] In this study we explicitly isolate the effect of KA by studying the $J=0$ case for various dopings.

Beginning at a doping of only a single hole in the infinitely correlated system, we track the effect of KA into the intermediate doping regime. The specific heat develops a low-temperature peak indicative of effective spin interactions, generated by a dressed hole in an AFM-spin background. The same effect is manifest in the susceptibility results where we present an x- and J-dependent effective interaction, with a small but finite AFM value in the case of $J=0$. We proceed by an explicit computation of the frequency-dependent Hall coefficient. The results show weak frequency dependence of R_H and encourage the applicability of its high-frequency limit R_H^* to practical situations. While small in magnitude compared to the spin susceptibility, we show through an identity in terms of derivatives—suggested by our numerical results—that the diamagnetic susceptibility alone may be closely connected to the temperature-dependent Hall coefficient.

This paper has two main objectives: We have recently studied the origin of the Curie-Weiss phase in Ref. 11 by

presenting the numerical results of the t-J model as applied to NCO. In this, the companion long paper, we provide fuller details of our results. Second, we will discuss the finite temperature t-J model starting from the Nagaoka regime and then extend into finite dopings. The structure is as follows: In Sec. II we describe our model and the exact diagonalization technique, which we utilize for our computations. We show details of the relevant finite clusters and the inclusion of a small magnetic field perpendicular to the two-dimensional planes. Section III presents the results for the static properties: Sec. III A, chemical potential; Sec. III B, specific heat and entropy, as well as Sec. III C, the spin susceptibility. We point out the implications of electronic and spin frustration for the temperature and doping dependence of these quantities. We then investigate in Sec. III D the dynamic Hall coefficient $R_H(\omega)$ and compare its dc and high-frequency behavior. Last, in Sec. III E we draw a connection between the Hall coefficient and the diamagnetic susceptibility as a relation between derivatives. For all properties, we study systematically the dependence on temperature, doping, and interaction strength. In Sec. IV we conclude and summarize our results.

II. MODEL AND EXACT DIAGONALIZATION

As a model for hole doped strongly interacting Mott insulators, the t-J Hamiltonian can be applied to the experimental situation of electron-doped NCO after an electron-hole transformation,[12] making use of the symmetry of the Hubbard model in respect to half filling. The replacement rules are $t \to -t$, $\delta = |1-n| = x$, and $q_e \to -q_e$, where δ (x) always refers to hole (electron) doping away from half filling and n is the electron density per site. This leads to the t-J model

$$\hat{H} = -t \sum_{\langle i,j\rangle,\sigma} \hat{P}_G \hat{c}^\dagger_{i\sigma} \hat{c}_{j\sigma} \hat{P}_G + J \sum_{\langle i,j\rangle} \left(\hat{S}_i \cdot \hat{S}_j - \frac{\hat{n}_i \hat{n}_j}{4} \right), \qquad (1)$$

where $\hat{c}^\dagger_{i\sigma}$ ($\hat{c}_{i\sigma}$) creates (annihilates) an electron of spin σ, $\hat{S}_i$ is the three-component spin-operator, $\hat{n}_i$ is the number operator and i specifies the lattice site. $\hat{P}_G$ denotes the Gutzwiller projector and the summation is over all nearest-neighbor pairs $\langle i,j\rangle$.

In the following, whenever doping x is mentioned this refers to electron doping in the NCO system and hole doping in the model Hamiltonian. To compute the complete spectrum—as required for thermodynamic properties—we employ the canonical ensemble exact diagonalization technique for small clusters. The computational demand limits the analysis to quite small systems and finite-size effects are challenging to overcome. Nonetheless, careful comparison between several systems of different geometry enables us to extract the stable behavior and somewhat isolate finite-size effects. Conversely, finite-size effects can help identify the favored eigenstate of a system.

We have employed several toroidal and ladder geometries with L=9, 12, and 18 sites, as well as the highly symmetric icosahedral geometry. The icosahedron—a 12-sited platonic solid with 20 equilateral triangular faces—shares the property of geometric frustration with the infinite system while the effect of the reduced coordination number (z=5) appears to have only a small, quantitative effect on the computational results [Fig. 1(c)]. Our 12-site torus clusters are depicted in Figs. 1(a) and 1(b). A third 12-site cluster is the simple 4×3 cluster (called torus c, not pictured).

While the numerical effort of exact computations for translationally invariant systems can be significantly reduced by exploiting space-group symmetries of the Hamiltonian, these symmetries are broken upon the introduction of a magnetic field, as relevant for the evaluation of the Hall coefficient. A magnetic field is introduced by the usual Peierls substitution which modifies the hopping t between sites i and j by

$$t \to t_{ij}(\mathbf{A}) = t \exp\left(i \frac{2\pi}{\phi_0} \int_i^j \mathbf{A} \cdot d\mathbf{s} \right), \qquad (2)$$

where $\mathbf{A}$ is the magnetic vector potential and ϕ_0 is the flux quantum. We define the flux threading a triangular plaquette as $\alpha \equiv \frac{2\pi}{\phi_0} \oint_\Delta \mathbf{A} \cdot d\mathbf{s}$. In finite systems, the value of the smallest nonzero magnetic field is limited to values of $\alpha \geqslant \pi/l$ where l is the length of a periodic loop in the system. Through a particular gauge we can achieve l equal to the number of triangular faces in the cluster, this guarantees the equality of the flux values through all plaquettes. An example is given in Fig. 1(a). A similar strategy has been followed in the case of the square lattice quantum Hall effect.[13] We complement the computations on periodic systems with ladder systems, which enable an infinitesimal flux to be chosen due to open boundary conditions in one of the spatial dimensions [Fig. 1(b)] and the Landau gauge is adequate. In the case of the icosahedron [Fig. 1(c)] the magnetic field is applied through a (fictitious) magnetic monopole in its center, creating equal magnetic fluxes through all triangular plaquettes.

III. RESULTS

A. Chemical potential

The chemical potential is evaluated as a derivative of the free energy F with respect to the particle number N,

$$\mu(T) = \frac{\partial F(T)}{\partial N}.$$

The derivative has to be taken as a discrete difference of $F(N)$. To take this derivative numerically, we use the central difference formula. Hence it is suitable to define

$$\mu^+ = F(N+1) - F(N) \text{ and } \mu^- = F(N) - F(N-1).$$

The value of μ can then be obtained from

$$\mu = \frac{(\mu^+ + \mu^-)}{2}.$$

In Figs. 2(a) and 2(b) we present $\mu(T)$ at several J and dopings x. At low temperatures $\mu(T)$ shows degenerate Fermi behavior ($\propto T^2$).[14] In the strong-correlation regime (J=0 and J=0.4$|t|$) the ground-state (g.s.) internal energy has a

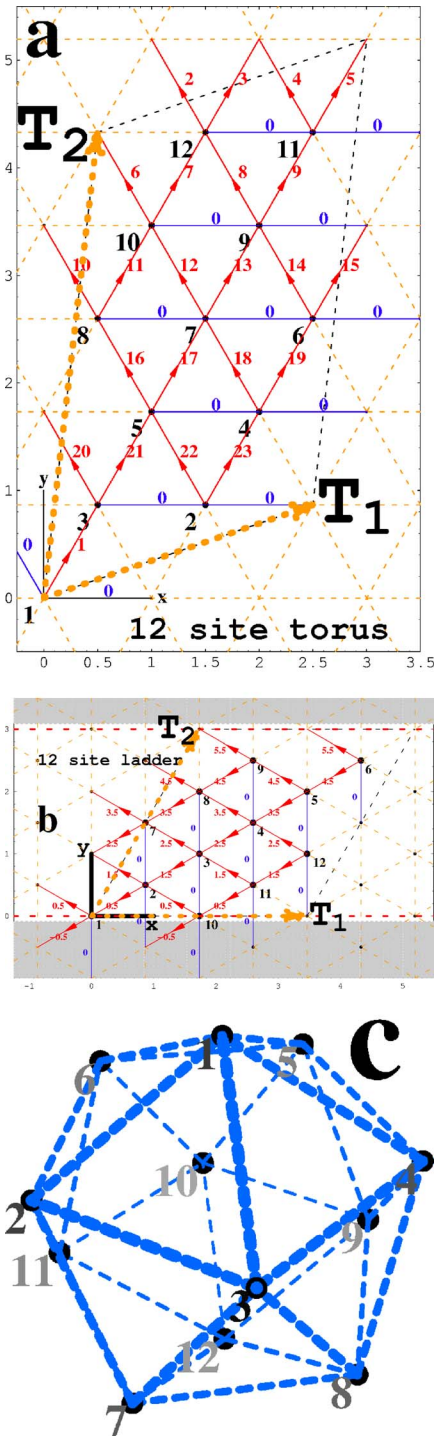

FIG. 1. (Color online) Small numbers along arrows (red) denote Peierls phases in units of the flux through a single plaquette, phases on icosahedron (c) not shown for clarity. Dotted parallelograms (black) specify boundaries of finite clusters (a) and (b). All sites on corners of parallelograms are equivalent and translations along bounding vectors $\mathbf{T}_1$ and $\mathbf{T}_2$ tile infinite lattice; shaded region in (b) forbidden for ladder. Note: different coordinate systems are used for torus and ladder. For ladder system we use the Landau gauge with $\mathbf{A} \propto y\hat{x}$, (a) represents only one choice (denoted torus a) for 12 sites. Another (denoted torus b) results from ladder (b) by connecting all corners through $\mathbf{T}_1$ and $\mathbf{T}_2$ (not shown). Torus c is simple 3×4 cluster (not shown).

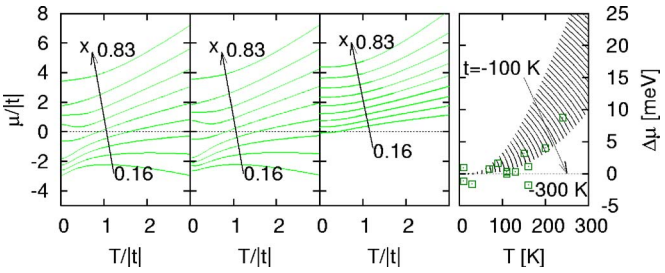

FIG. 2. (Color online) Chemical potential $\mu(T)$ for all accessible dopings on torus b: $x=2/12=0.16$ to $10/12=0.83$ for $J=0$ (a), $J=0.4|t|$ (b), and $U=0$ (c). Data for $U=0$ computed for infinite noninteracting system, comparison with (a)–(c) shows relatively weak effect of interactions in the doping range $x>0.8$. (d) Squares are experimental data for $\Delta\mu(T)=\mu(T)-\mu(0)$ from Ref. 15 Shaded area is a comparison with our data for $U=0$ for $t=-100$ K to $t=-300$ K.

maximum at intermediate dopings $x \approx 0.5$ due to the competition of increasing number of mobile particles and reduction of the available vacancies upon decrease of doping and hence the low-temperature chemical potential changes sign here. In the high-temperature regime the doping dependence of the Hilbert-space dimension determines the limit of

$$\mu(T \to \infty) \propto T \frac{\partial g(x)}{\partial x}$$

with $g(x)=(1-x)\ln[2x/(1-x)]+\ln(1/x)$ essentially the natural logarithm of the dimension of the Hilbert space. In the projected t-J model, $g(x)$ peaks at $x=1/3$. For $x<1/3$ the slope at large T becomes negative. In Fig. 2 the comparison of $\mu(T)$ for different interactions shows that the impact of projected fermions near half filling is to force a negative slope of μ for $x>0$ which occurs in the noninteracting system only for $x<0$. This is an example of the qualitative difference between a strongly interacting Fermi system and its noninteracting counterpart.

At larger $x>0.7$ the effect of strong interactions is gradually lost and the temperature dependence resembles that of the noninteracting Fermi system [Fig. 2(c)]. For low temperatures well below the linear range of μ, finite $J>0$ generally increases the value of the chemical potential with a stronger increase for x near the Mott insulator. The high-temperature behavior is independent of J.

In Fig. 2(d) we compare the results with direct experimental measurements of the T-dependent chemical potential[15] at $x \approx 0.83$. Since our results in this doping range are rather insensitive to the value of U, we compare with our $U=0$ results. Here, $\mu(T)$ was obtained directly from the tight-binding density of states by the implicit equation $\langle n \rangle = 2 \times \int_{-\infty}^{\infty} f(\epsilon,\mu)\rho(\epsilon)d\epsilon$ with fixed $\langle n \rangle = 1+x$, where f denotes the Fermi-Dirac distribution function and ρ is the noninteracting density of states. This fit confirms the notion of NCO as a system with an unusually small Fermi temperature scale. In Fig. 2(d) we show as a shaded region the values $t=-100$ K to $t=-300$ K, photoemission results[8] point to a value of $|t| \approx 10$ meV ~ -118 K, hence $|t|$ here is more than an order of magnitude smaller than in the cuprate supercon-

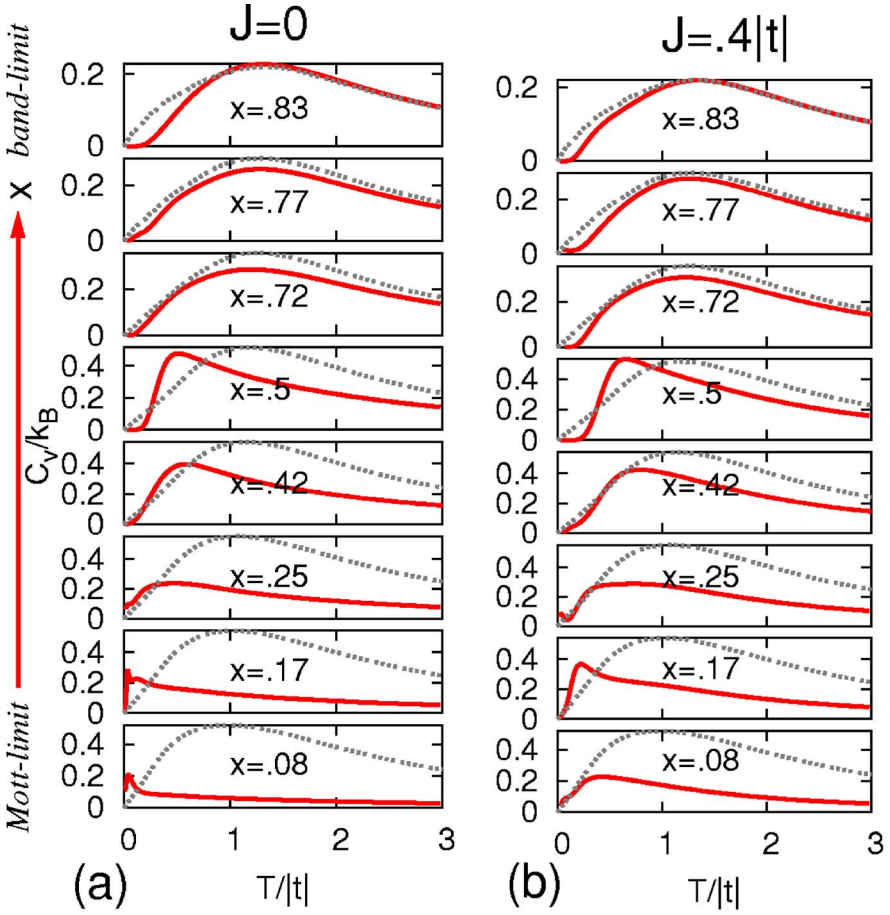

FIG. 3. (Color online) Specific heat per site as function of T for varying x, computed on 18-site ($x \geqslant 0.72$) and 12-site cluster ($x < 0.72$), (a) $J=0$, (b) $J=0.4|t|$. Dotted lines show $C_v(T)$ for noninteracting fermions and solid line for exact results. Note: scale changes in plots of different dopings, long temperature exponential behavior at large x due to finite-system induced gap in energy spectrum. Results for $x=0.72$ appeared in Ref. 11.

ductors. In the following, when making contact with experiments, we take $t=-100$ K for simplicity.

B. Specific heat, entropy

In Figs. 3(a) and 3(b) we present the specific heat per site,

$$C_v(T) = \frac{1}{L}\frac{d\langle E\rangle}{dT},$$

with $\langle E\rangle$ the thermodynamic expectation value of the internal energy. We first concentrate on the case of $J=0$, corresponding to an infinite on-site interaction. Near the band insulator ($x \approx 1$) the temperature dependence resembles that of noninteracting fermions, computed at fixed particle density by first determining $\mu(T)$ and then the T derivative of the internal energy. When the doping is reduced, the main energy scale—manifest in a peak of $C_v(T)$ at temperature $T_m(x,J)$—continuously moves to smaller temperatures, away from the tight-binding peak. Even at our lowest doping $x=1/L$ the peak feature persists (called the KA peak). This feature is magnified in Fig. 4 for several different systems.

Numerical work on the g.s. of the problem of a single hole in an AFM spin background[2] suggests this system to exhibit a weak effective AFM interaction $J_{eff} \propto 1/L$ due to the projected kinetic energy term only. While for one hole this excitation decays in the thermodynamic limit, J_{eff} nonetheless induces a Néel ordered AFM g.s. and low-energy excitations similar to those observed in the HAF.[9]

The validity of our computations for the case of a single hole is underscored by the entropy. In Fig. 5, the temperature dependence of the entropy shows that the low-energy features observed in the specific heat are necessary for the entropy to obtain its (known) high-temperature limit. For $T/|t| \approx 0.075$ half the entropy is recovered [$s(T)/s(\infty)=0.5$], indicative of entropy enhancement due to electronic frustration.[16] For intermediate dopings, the entropy reaches half its maximum at $T/|t| \approx 0.75$ and for dopings $x \approx 0.7$—relevant to the Curie-Weiss phase of NCO—we find $T/|t| \approx 0.78$.

Within a high-temperature expansion[16] a numerical argument was given for an S-shaped low-temperature behavior of

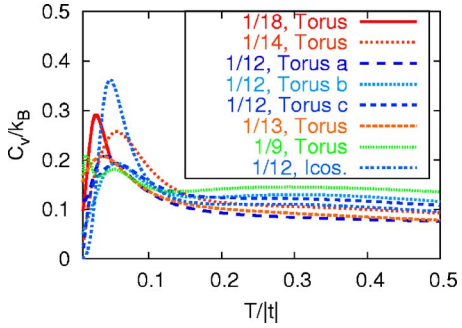

FIG. 4. (Color online) $C_v(T)$ at $x=1/L$ for several sets of boundary conditions, peak in specific heat is system-independent property.

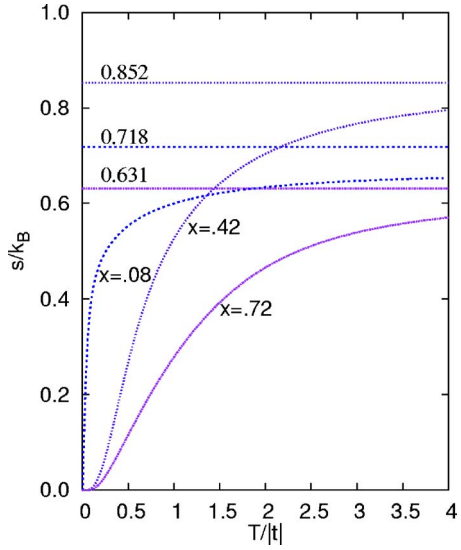

FIG. 5. (Color online) Entropy per site for three different dopings at $J=0$ ($x=1/12=0.08$, $x=5/12=0.42$, $x=13/18=0.72$), horizontal lines indicate high-temperature limit $s(T\to\infty)=k_B\ln(g(x))/N$, $x=0.08$ corresponds to Fig. 4. Exponential increase at low T for intermediate x due to finite system-size gap Δ.

the entropy for the case of $x=0.2$ and $x=0.4$. Our computations at small dopings rather suggest $s\sim T$ for low T as applicable to a metal from Fermi-liquid arguments. It is remarkable here that $C_v(T)$ reflects these low-energy excitations, notably even for larger dopings than the one applicable to the Nagaoka situation.

We now distinguish the effect of $J>0$ [Fig. 3(b)]. This scenario has been investigated by several authors for the case of the hole doped square lattice and the HAF.[17,18] For the situation of a single hole $J>0$ shifts the KA peak to larger temperatures $T_m=J/t$. In Fig. 8(b) we present the peak positions as function of doping and J. We find $T_m(x,J)$ to *increase* monotonically both with x and J and the slope as function of J for fixed x to decrease for larger values of x. Extrapolating these results at a given value of J to $x=0$ we obtain roughly $T_m(x=0)\approx J$. Our result should be distinguished from investigations on the $t>0$ square lattice,[17] where T_m was found to follow the opposite trend *decreasing* slightly with x at small dopings, along with a rapid suppression of the peak. This supports the notion of electronic frustration contributing to AFM correlations in the present study in opposition to competing AFM exchange coupling and the FM Nagaoka mechanism in the case of $t>0$, capable of quickly eliminating the low-energy spin excitations.

An experimentally interesting quantity related to the specific heat is γ defined by $C_v(T)\sim\gamma T$ or $\gamma=ds/dT$ corresponding to the low-energy electronic part of the specific heat. When extracting this quantity from our numerical results, we neglect the contributions at very low T arising purely from the finite system induced gap in the spectrum [scaling as $\exp(-\Delta/T)$ where Δ is the gap between the g.s. and the first excited state]. For the large doping case $x=0.7$ we found[11] $\gamma\approx 45(\pm 5)$ mJ/mol K^2 ($\gamma_0\approx 33$ mJ/mol K^2 for noninteracting tight-binding electrons), indicating a significant many-body enhancement. Experimental results[19] indicate $\gamma\approx 26$ mJ/mol K^2. On the other hand, in the low-doping regime the linear increase with T is only observed in a very small temperature range and this range is possibly better classified as a non-Fermi-liquid regime. Roughly, $\gamma(x)/\gamma_0(x)\gg 1$ for $x\gtrsim 0$. The increase in γ with decreased doping is also demonstrated clearly by the low T slope of $s(T)$ in Fig. 5.

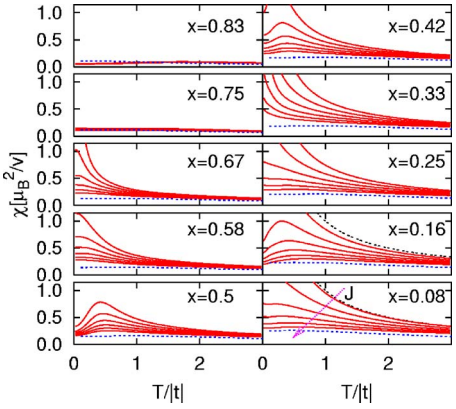

FIG. 6. (Color online) Spin susceptibility per site $\chi(T)$ for all accessible dopings x on 12-site torus. Dependence on $J/|t|=(0,0.1,0.2,0.3,0.4,0.5)$, indicated by arrow, blue dotted line shows bare susceptibility for noninteracting fermions of density $n=1+x$ and black dotted line indicates susceptibility of isolated spin-$\frac{1}{2}$ fermions of density $n=1$. Plots for $x\geqslant 0.58$ appeared in Ref. 11.

C. Spin susceptibility

To gain further insight into the role of spin fluctuations and to address the existence of the experimentally observed Curie-Weiss phase of NCO,[20] we compute the spin susceptibility $\chi(T)$ as function of temperature from the Gibbs free energy $G(T,M)$, here $M=\Sigma_i S_i^z$ is the total magnetization. This quantity follows from the Helmholtz free energy $F(T,H)$ through a Legendre transformation $G(T,M)=F(T,M)-H\frac{\partial F}{\partial H}=F(T,H)+MH$. H is the externally applied magnetic field;

$$\chi^{-1}=\frac{d^2G}{dM^2}$$

can then be evaluated numerically, by constraining the canonical ensemble to the sector of minimal $|S_z^{tot}|$, and those sectors where S_z^{tot} is raised (lowered) by $\hbar$.

For low temperatures, near the band limit ($x=1$) we identify weakly temperature-dependent, Pauli-like behavior of χ, reminiscent of the experimentally observed spin-density wave (SDW)-phase (Fig. 6). When x is lowered past $x=0.75$ we find[11] a crossover to a Curie-Weiss-like behavior with appreciable renormalizations of the g.s. susceptibility compared to its bare value, mirroring the experimental findings. This behavior can roughly be understood by picturing electrons distributed on an empty lattice: Initially, the many-body eigenstate enables the electrons to move around without interacting directly with their neighbors, yielding a susceptibility that is J dependent only to second order. When the

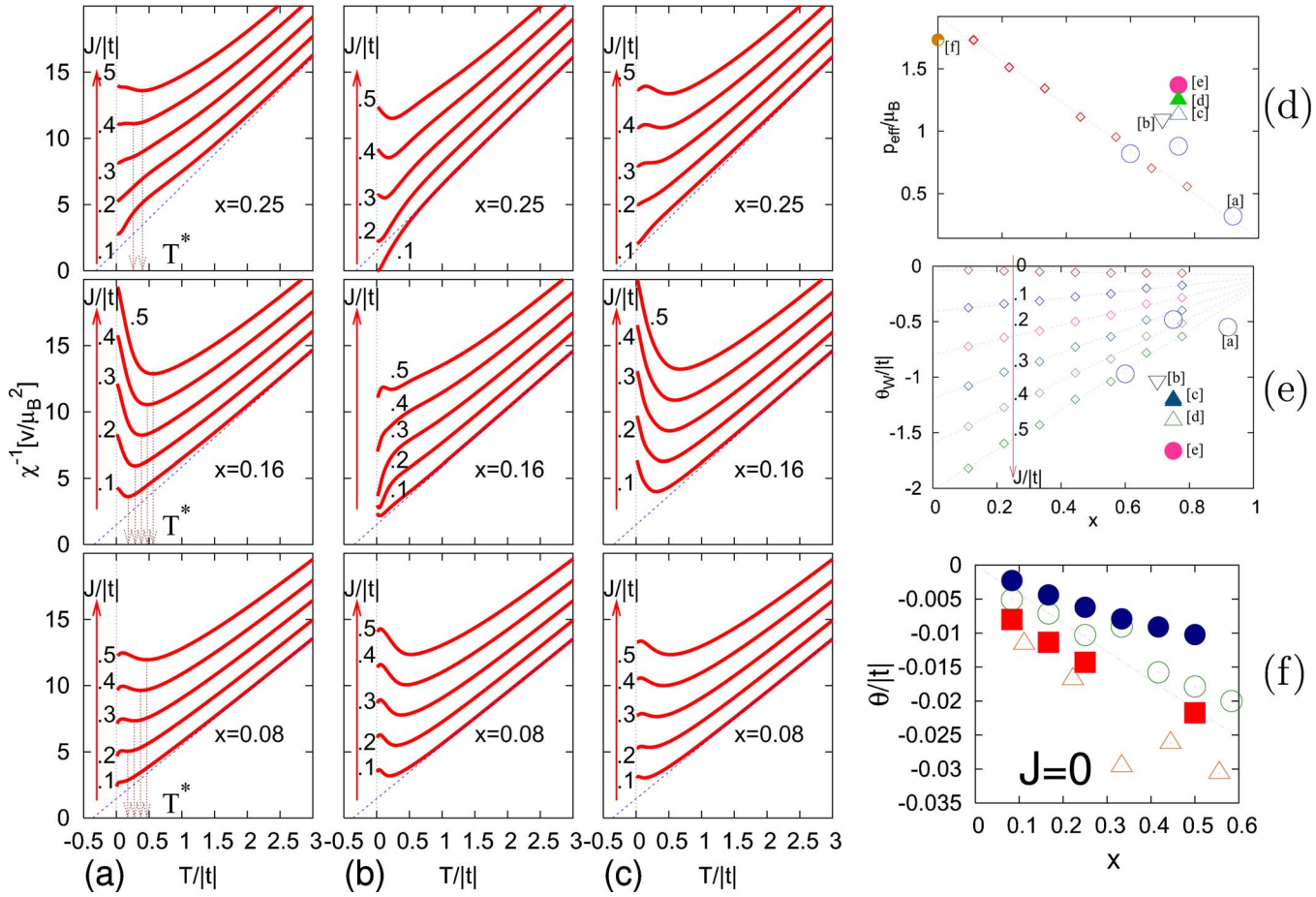

FIG. 7. (Color online) (a)–(c) Inverse susceptibility vs temperature for dopings $x=1/12=0.08$ (bottom), $x=2/12=0.16$ (center), and $x=3/12=0.25$ (top) for torus a, b, and c (left to right). Solid vertical arrows show increase in J, dotted (blue) line shows example for fit to extract Weiss temperature $\theta(x,J)$ and effective moment p_{eff}. Dotted vertical arrows indicate temperature T^*; Note: comparison of the three systems allows isolation of finite-size effects, most visible for $x=0.16$. (d) Effective magnetic moment p_{eff}. (e) Weiss temperature θ vs doping x for $J=0\ldots0.5$. Letters in angled brackets correspond to experimental data from (a) Viciu *et al.* (Ref. 21), (b) Gavilano *et al.* (Ref. 22), (c) Sales *et al.* (Ref. 23), (d) Takeuchi *et al.* (Ref. 24), (e) Motohashi *et al.* (Ref. 19), and (f) effective moment of isolated spin-$\frac{1}{2}$-particles on half filled lattice. (f) Magnification of θ vs x for $J=0$ for several clusters.

density is increased ($n>0.25$ or equivalently $n<1.75$), electrons are forced to interact through the exchange-coupling directly and hence yield a strongly J-dependent magnetic susceptibility. The emergence of the Curie-Weiss phase is further supported by the strong magnetic-field suppression of the Heikes-Mott term in the thermopower within the t-J model, an effect due to spin entropy[5] as was demonstrated in Ref. [11].

For temperatures larger than a certain crossover temperature (which we call T^*), for all dopings, $\chi(T)$ can be described through the Curie-Weiss form

$$\chi(T) = \frac{1}{3}\frac{L}{V}\frac{\mu_B^2 p_{eff}^2}{k_B(T-\theta)}$$

with the Weiss temperature θ and the effective magnetic moment p_{eff}, V is the volume of the crystal, and L is the number of sites. For all accessible system sizes—in particular torus a, b, c (Fig. 1)—we compute $\chi(T)$ to extract θ, p_{eff} and T^*, the parameters characterizing the magnetic properties at a given doping and interaction strength. To determine θ and p_{eff} we fit the high-temperature part of our computations for $\chi(T)$ to the function $f(T)=a/(T-b)$ [compare Fig. 7(a)]. In Figs. 7(a)–7(c) we present the inverse susceptibility at several different dopings near the Mott-insulating phase. The results for θ and p_{eff} are shown in Figs. 7(d)–7(f). For all x and $J\geqslant 0$, θ remains negative indicating AFM correlations. θ shows a linear increase when the doping is increased or the interaction is decreased. In short, as mentioned in Ref. 11, θ can be collapsed into the form $\theta(x,J)=-cJ_{eff}(x)$ where

$$J_{eff}(x) = J(1 + c''x|t|) + c'x|t|$$

with $c=4.0$, $c'=0.014\,25$, and $c''=-0.9175$. In contrast to the relation given by Anderson *et al.*[1] in the case of the $t>0$ square lattice, in our situation of $t<0$ even at $J=0$ there is a slightly *negative* intercept suggesting AFM spin interactions in the low-temperature regime of the electronically frustrated $U=\infty$ Hubbard model, indicative of *kinetic antiferromagnetism* (KA).

On the other hand, once $J>0$ is allowed, this intercept grows strongly and expresses dominant AFM correlations [Fig. 7(e)]. We compare these results with experiments for various dopings ($x>1/2$) of NCO. Among others, the cases of $x=0.75$,[19,23,24] $x=0.7$,[22] $x=0.6$, and $x=0.9$,[25] various x in the three-layer system[21] and $x=0.55$ (Ref. 26) were experimentally investigated. The comparison with experiment proves difficult due to the large number of structural phases,[21] the role played by the Na ions in the crystal, and the large quantitative and qualitative difference between powder and single-crystal samples.[23] However, the Weiss temperature appears to lie between 100 and 200 K near $x=0.7$ [varying considerably with $H\|\mathbf{c}$ and $H\|\mathbf{a}$ (Ref. 23)] and was measured to be smaller at larger dopings.[21] Hence at least for $x>0.5$ the t-J model description yields reasonable experimental agreement.

The effective magnetic moment p_{eff} in units of μ_B has a value close to that obtained for localized spin-$\frac{1}{2}$ particles at half filling $\mu_{1/2}=g\times\sqrt{s(s+1)}=\sqrt{3}$ and decays linearly for $x\to 1$.

The inverse susceptibility shows a minimum at a temperature T^* which becomes more pronounced with increasing J. At low temperatures the system prefers antiferromagnetic order which is *strengthened* by $J>0$. Thermal spin fluctuations break this order and when T is increased to values of order J a small perturbative B field is sufficient to align spins antiparallel to the field. Hence the susceptibility is largest at this temperature. When T is further increased, the ability of the field to flip spins is weakened by thermal fluctuations, consequently, $\chi(T)$ decreases. The behavior of this peak as function of hole doping away from the Mott insulator has already been investigated within a high-temperature expansion.[16]

Due to the small size of the systems available to our study, it is difficult to confirm the results for the doping dependence.[16] Here, we study the behavior as function of J, considering several dopings near half filling and several system geometries [Fig. 8(a)]. The figure indicates that $T^*/|t|$ roughly scales as $J/|t|$ hence the scale at which the system undergoes a transition from an AFM-ordered to a paramagnetic state is set by the interaction strength. As was shown for the case of $J=0$ and $t>0$ in the hole doped system,[2] a single hole favors AFM Néel order and numerical results[9] indicate that the triangular lattice Heisenberg model also favors Néel order—at least in the g.s. and the elementary excitations—hence it is not surprising that a finite $J>0$ emphasizes this tendency. This is in opposition to the case of $t<0$ where the kinetic energy term favors ferromagnetism and competes with the Heisenberg interaction preferring AFM.

D. Hall coefficient

Experimentally, NCO has been shown to exhibit unusual thermoelectric properties, resulting from strong electron correlations. Wang *et al.*[6] measured the dc-Hall coefficient as a function of temperature at several dopings showing unexpected temperature dependence with an oscillatory behavior below 200 K and a rapid linear increase for temperatures above 200 K.

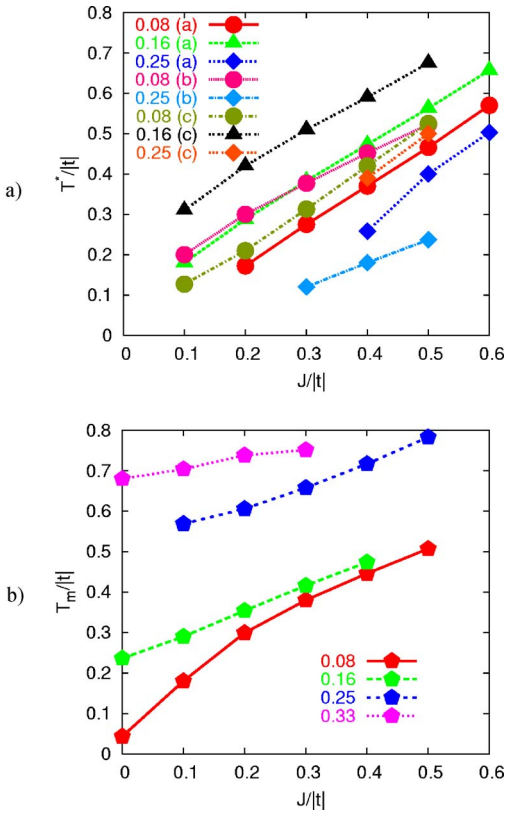

FIG. 8. (Color online) (a) AFM-paramagnetic crossover temperature as function of J for several dopings on 12-site torus clusters a, b, c. (b) Evolution of T_m as function of J, values averaged over three 12-site clusters a, b, c.

Much theoretical work has been invested into the study of R_H on square lattices[3,12,27–39] both for g.s. properties and for finite temperatures. For the triangular lattice, it was possible to predict the high-temperature behavior within a high-temperature expansion of the t-J model[3,12] in its high-frequency limit. Several authors have also attempted to describe this behavior through Boltzmann transport theory[36,37] within the relaxation time approximation, where R_H is expressed as an integral over the Fermi-surface curvature and the relaxation time τ_k is taken to be isotropic. For large dopings—$x\geqslant 0.7$—where the holelike Fermi surface of NCO approximates a circle, this leads to the same high-temperature linear coefficient as the t-J-high-temperature expansion, however, the behavior completely diverges in the dense regime ($x<0.7$), possibly due to the misleading replacement of the interacting Fermi surface by its noninteracting counterpart. Also, at low temperatures—where the relaxation time is anisotropic—the oscillatory behavior seen in experiments is not reproduced.

To shed some light on the low-temperature and strongly correlated behavior, we start from the high-frequency limit[3] for $R_H(T,\omega)$:

$$R_H^*(T) \equiv \lim_{\omega\to\infty} R_H(T,\omega) = \lim_{B\to 0}\left(-\frac{ivL}{Be^2}\frac{\langle[J_x,J_y]\rangle}{\langle\tau_{x,x}\rangle^2}\right). \quad (3)$$

Here, e is the electron charge, J_x (J_y) are the currents in x (y) directions, v is the unit-cell volume, and $\tau_{x,x}$ is the diag-

onal part of the stress tensor. To ensure the effect of strong correlations within this limit, it is necessary to force the hierarchy $t<\omega\ll U$. We enable this by projecting out double occupancy using the Gutzwiller projector, hence the t-J model is the appropriate description.

Our plan is as follows: we show the connection of this high-frequency limit—not measurable in experiments—to the dc or low-frequency behavior. Then we evaluate the dependence on the parameters T, J, and x for several systems. Hence for the first part we compare R_H^* with the expression derived from the Kubo formulas for the electrical conductivities

$$\sigma_{\alpha,\beta}=\frac{ie^2}{\omega v}\left(\langle\tau_{\alpha,\beta}\rangle-\frac{1}{Z}\sum_{\mu,\nu}\frac{\exp-(\beta\epsilon_\nu)-\exp-(\beta\epsilon_\mu)}{\epsilon_\mu-\epsilon_\nu-\omega-i\eta}\langle\nu|J_\alpha|\mu\rangle\right.$$
$$\left.\times\langle\mu|J_\beta|\nu\rangle\right), \tag{4}$$

with ϵ_ν the νth energy eigenvalue of $\hat{H}$ and Z the canonical partition function. In terms of this expression the Hall coefficient is given by

$$R_H(\omega)=v\frac{\partial}{\partial B}\left(\frac{\sigma_{x,y}(\omega)}{\sigma_{x,x}(\omega)\sigma_{y,y}(\omega)}\right)_{B=0}. \tag{5}$$

As a transport object R_H is a demanding quantity to study on finite clusters. The effect of boundary conditions and their finite-size implications are difficult to eliminate. We introduce a small magnetic field through the Peierls substitution [Eq. (2)] which impacts only on the orbital motion of the electrons and does not couple to the spin. Studying R_H on toroidal and spherical geometries reduces the finite-size effects on the transport, however, these periodic systems constrain the smallest accessible flux ϕ_0 to π/L. For $L=12$ this is already a considerable flux. An alternative are ladder systems such as in Fig. 1(b) where the limit $\phi_0\to 0$ is possible. However, ladders have additional finite-size effects impacting on the transport quantities.

For several dopings ($x=0.08,0.67,0.75,0.83$) we compute $R_H(\omega)$ as a function of temperature both on the torus and the icosahedron. To take into account the finite size of the system, a broadening η of the energy equal to the mean level spacing of the current matrix elements was employed, this requires $\eta\approx 3|t|$. In Fig. 9 we show R_H as a function of temperature at three different frequencies. Comparing $\omega=0$ to $\omega=\infty$ we find that the dc limit is qualitatively the same as the high-frequency limit, however, the overall temperature dependence is scaled by a renormalization factor $s\equiv R_H(T,\omega=0)/R_H(T,\infty)$ where s is only weakly temperature dependent. For the torus, s was found to be 0.83 (0.78) at $x=0.83$ ($x=0.75$). At $x=0.083$ the many-body renormalization is stronger.

Conversely, in Fig. 10 we show the frequency dependence of R_H at several temperatures and different dopings. Similar to the work done by Grayson *et al.*[40] on the Hall angle, finite frequency experiments may be helpful to confirm the weak frequency dependence seen in our computations: With $|t|\approx 10$ meV results in the frequency range $\omega\geq 3|t|\approx 30$ meV could be compared to our theoretical results and hence

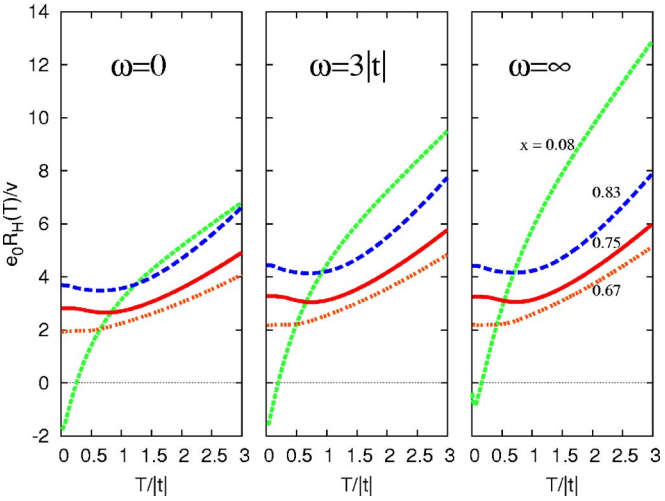

FIG. 9. (Color online) $R_H(\omega,T)$ on 12-site torus at several frequencies for several dopings and $J=0$.

lend experimental support for the usefulness of the high-frequency limit[3] of R_H.

We have computed two additional quantities related to the dc limit as checks of the validity of the dc computations. Zotos *et al.*[29] derived an expression for the g.s. expectation value, $R_H(T=0)=\frac{1}{|e|}\frac{d}{dn}\ln D(n)$ with D the charge stiffness $D=\frac{d^2\langle E\rangle_0}{d\phi^2}$, $\langle E\rangle_0$ the g.s. energy, and ϕ a constant flux inducing a persistent current.[41] In this fashion, we evaluated the doping dependence of the g.s. and found $R_H^0>0$ in the experimental regime near $x\approx 0.7$ and a divergence $R_H^0\to-\infty$ as the Mott limit is approached.[11] The second check refers back to the basic definition of the dc-Hall coefficient $R_H=-E_y/(Bj_x)$ and computing this directly on a ladder system. This computation showed no change of sign for $x\approx 0.7$ as a function of T and a qualitatively similar behavior to the $\omega=\infty$ result.

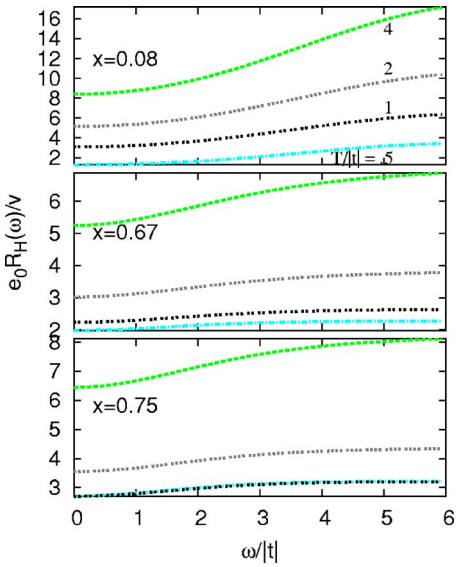

FIG. 10. (Color online) $R_H(\omega)$ at several temperatures and dopings as function of frequency on 12-site torus a for $J=0$. Temperatures in all plots $T/|t|=(0.5,1,2,4)$.

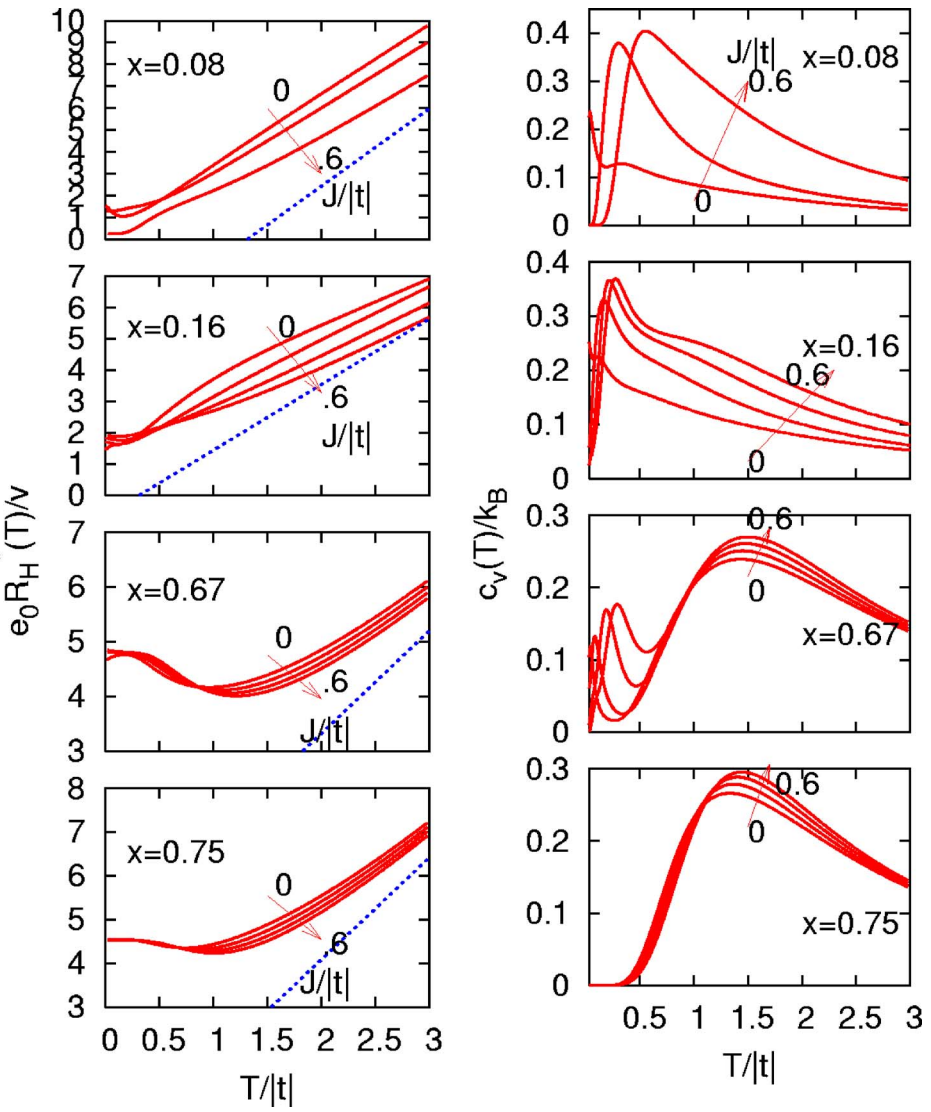

FIG. 11. (Color online) (left) $R_H^*(T)$ for several x and J for torus b. (right) $C_v(T)$ for several x and J on same torus.

Encouraged by the notion of weak frequency dependence, we studied $R_H^* \equiv R_H(\omega=\infty)$. We have studied several 12 site tori, several doping values on an 18 site torus, the icosahedron and several ladders.

The g.s. $R_H^*(x)$ shows a Drude dropoff near the band insulator and a saddle point around $x=0.5$ as was reported by the authors in Ref. 11. When the strong-correlation regime near the Mott insulator is approached ($x<1/2$), the slope again increases and for 1 hole ($x=0.083$) R_H^0 changes sign.

The high-temperature behavior confirms the prediction from the high-temperature series expansion.[3,12] The interesting temperature range is for $T<2|t|$ where the experimental data show an oscillatory behavior and analytical results are not available (Fig. 11). Our computations show a distinct minimum in $R_H(T)$ which appears near $T=|t|$ in the Curie-Weiss regime ($x\approx 0.7$) and continuously moves to smaller temperatures as the doping is decreased. For the smallest dopings accessible ($x=1/L$) this minimum appears near $T=0.2|t|$, while the behavior becomes linear at higher T in all cases. In the Curie-Weiss regime some systems also show a weak maximum close to $T=0.25|t|$. These results point towards the existence of two distinct energy scales. The pronounced minimum appears to be correlated with the peak in the electronic specific heat (Fig. 11), which also occurs around $T=|t|$ in the band limit, and gradually shifts towards smaller temperatures with decreased doping.

To strengthen this point it is useful to include the dependence on J. As reported for the specific heat, the effect of J is to move the peak in specific heat to larger temperatures. This behavior is mirrored by R_H. In Fig. 11 we show $R_H(T)$ for several dopings and J. At $x=0.75$ the peak of $C_v(T)$ shifts from $T=1.3|t|$ to $T=1.5|t|$ while the minimum in $R_H(T)$ moves from $T=0.75|t|$ to $T=1.1|t|$. At $x=0.67$ the behavior around $T=|t|$ is similar, however, an additional peak in the specific heat emerges at $T<0.5|t|$. A qualitatively similar feature is seen in other clusters, however, its magnitude is dependent on the system geometry. Hence we do not attempt to extract *quantitative* information in the T range below $T=0.5|t|$. Nonetheless, it is important to note that with decreasing doping a second energy scale—caused by spin interactions—becomes dominant. At small doping $x=0.16$ and $x=0.08$ the specific heat becomes strongly J dependent and the main peak in the specific heat—as discussed in the first section—increases significantly with J. The variations in $R_H(T)$ with J are also more pronounced.

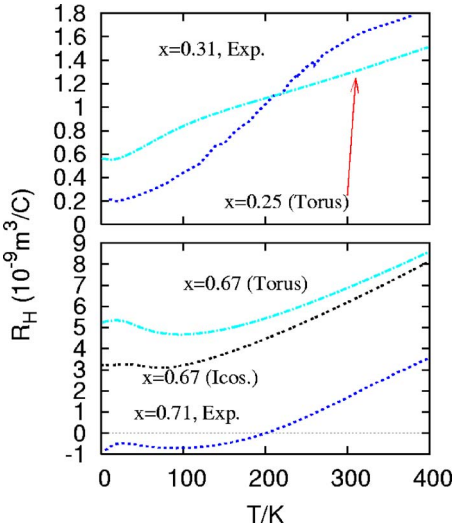

FIG. 12. (Color online) Comparison of 12-site torus b and icosahedron with experiment (Ref. 36) at $x=0.31$ and $x=0.71$, we take $t=-100$ K, in the lower plot our numerical results are scaled to match the slope of the linear part at $T>200$ K in the experimental results.

Assuming $t\approx-100$ K we compare our results to the experimentally available data[6] at $x=0.31$ and $x=0.71$, this was done in Ref. 11 for $x=0.71$. In Fig. 12 the comparison at $x=0.31$ shows good agreement for the slope at high T and reproduces the temperature scale for the minimum near 25 K. For $x=0.71$ the temperature scale for the minimum near 100 K is seen both in experiment and theory. The slope of the high-temperature limit differs by a factor of 4 and was adjusted in the plot for better comparison. Also, the theory does not show the change of sign as function of temperature. However, the oscillatory behavior below $T=100$ K and the onset of the linear increase for $T>200$ K agrees well with experiment. Hence the exact temperature dependence of R_H remains a challenging task—both on the theoretical and experimental side.

E. Diamagnetic susceptibility

Last, we study the orbital susceptibility per site,

$$\chi_d(T) \equiv -\frac{1}{L}\frac{\partial^2 F}{\partial B^2},$$

where F is the free energy and B is the magnitude of the perpendicular magnetic field. We define the dimensionless flux $\alpha=BA/\phi_0$ through a triangular plaquette with $A=\sqrt{3}a^2/4$ the area of the plaquette and a the lattice spacing. We get

$$\chi_d = -\frac{1}{L}\frac{\partial^2 F}{\partial \alpha^2}\left(\frac{\partial \alpha}{\partial B}\right)^2$$

It is useful to employ ladder systems as shown in Fig. 1(b). Defining $t=\hbar^2/2ml^2$ we have

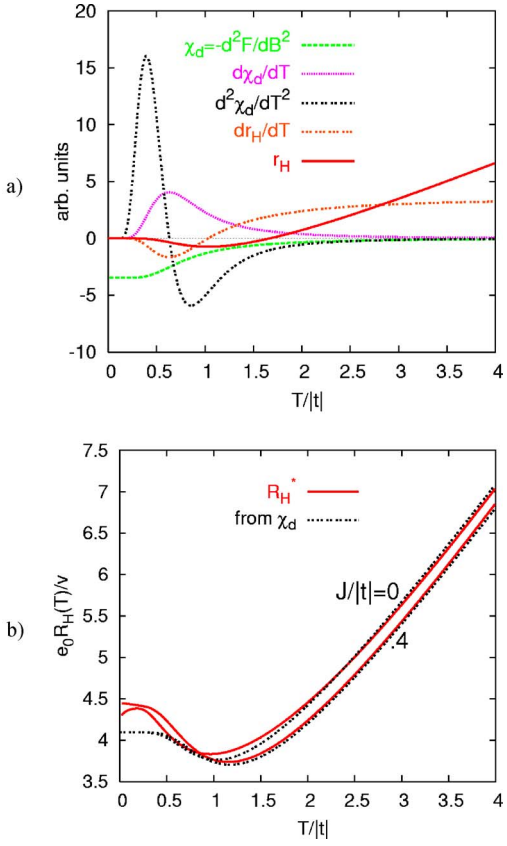

FIG. 13. (Color online) (a) $\chi_d(T)$ and unitless Hall coefficient r_H and their derivatives on a 12-site ladder at $x=0.83$. (b) Comparison of numerical results for $x=0.83$ for $R_H^*(T)$ (obtained on an 18-site torus) with the integral of Eq. (6) [$\chi_d(T)$ obtained on a 12-site ladder system] for two different values of J. Appeared partly in Ref. 11.

$$\frac{1}{L}\chi_d = -\frac{2m}{\hbar^2 l^2}A^2\mu_B^2\frac{1}{L}\frac{\partial f}{\partial \alpha},$$

where f is the dimensionless F/t and μ_B is the Bohr magneton. In Fig. 13(a) we present the diamagnetic susceptibility and its first two derivatives with respect to T. For free electrons in an infinite system, χ_d corresponds to electrons moving in circular orbits with radii inversely proportional to the magnetic field. R_H measures the polarization induced in a system with a stationary current and perpendicular magnetic field. It is hence reasonable to ask for a connection between these two quantities. Our numerics suggest the relation

$$T\frac{\partial^2 \chi_d}{dT^2} = c(x)\frac{\partial^2 R_H}{\partial T^2}, \tag{6}$$

where $c(x)$ is a function depending on doping x.

In Fig. 13(b) we display our numerical result for $R_H^*(T)$ at a doping relevant to the experimental situation[6] compared to the result obtained from integrating Eq. (6) and choosing the two integration constants appropriately. For $J=0$ this was done by the authors in Ref. 11 Ignoring the range for $T<0.5|t|$ which may be strongly influenced by finite-size effects, we find that both curves show a minimum at $T\approx|t|$

and then increase until $T=2|t|$. The reaction to finite $J>0$ is also similar for both curves, moving the minimum from $T=|t|$ to roughly $T=1.25|t|$. We plan to further investigate this connection within a high-temperature expansion for $\chi_d(T)$, in particular for the doping regime close to the Mott insulator.

IV. CONCLUSION

In summary, we have presented a systematic study of the entire doping regime for the triangular lattice *t-J* model with electronic frustration ($t<0$ for $n>1$). We have identified low-energy excitations, stemming purely from kinetic processes ($J=0$) of infinitely correlated spin-$\frac{1}{2}$ fermions. These are manifest in a peak structure in the specific heat emerging at very low T near the Mott insulator, however, persisting for intermediate dopings. The effect of electronic frustration is further supported by entropy enhancement in the underdoped regime with a low entropy recovery temperature.

We have studied both the diamagnetic and spin susceptibility. For the spin susceptibility we extract a relation for effective spin interactions $\theta(x,J)$ valid for all dopings. This stands in contrast to Anderson's formula for FM $t>0$, since in our case antiferromagnetism is *supported* rather than suppressed by doping. In the experimentally relevant doping range of $x>0.5$ we offer an explanation for the crossover between the Curie-Weiss and SDW metallic phases, as observed in experiments.[7] For the diamagnetic susceptibility χ_d a connection is obtained between χ_d and the temperature-dependent Hall coefficient.

The dynamic Hall coefficient reveals a weak frequency dependence and a qualitatively similar dc and high-frequency behavior, with stronger renormalizations close to the Mott limit. This strengthens the practical relevance of the high-frequency limit[3] R_H^*. The temperature dependence confirms the linear slope at high temperatures[3] and reproduces the experimentally observed minimum near $T=100$ K at $x=0.71$.

In conclusion, the *t-J* model is applicable to NCO for $x>0.5$ and shows that the interface of strong correlations and metallic behavior indeed describe the experimental situation here. For $x<0.5$ the frustrated *t-J* model leads to subtle effects of strong correlations, even in the case of $J=0$. Our results show that for the proper description of experimentally observed normal-state properties[7] there—such as the charge-ordered insulator at $x=0.5$ or the paramagnetic metal for $x<0.5$—an extension of the simple *t-J* model would be necessary.

ACKNOWLEDGMENT

This work was supported by Grant No. NSF-DMR0408247.

[1] P. W. Anderson, P. A. Lee, M. Randeria, T. M. Rice, N. Trivedi, and F. C. Zhang, J. Phys.: Condens. Matter **16**, R755 (2004).
[2] J. O. Haerter and B. S. Shastry, Phys. Rev. Lett. **95**, 087202 (2005).
[3] B. S. Shastry, B. I. Shraiman, and R. R. P. Singh, Phys. Rev. Lett. **70**, 2004 (1993).
[4] H. S. K. Takada, E. Takayama-Muromachi, F. Izumi, R. A. Dilanian, and T. Sasaki, Nature (London) **422**, 53 (2003).
[5] Y. Wang, N. S. Rogado, R. J. Cava, and N. P. Ong, Nature (London) **423**, 425 (2003a).
[6] Y. Wang, N. S. Rogado, R. J. Cava, and N. P. Ong, cond-mat/0305455 (unpublished).
[7] M. L. Foo, Y. Wang, S. Watauchi, H. W. Zandbergen, T. He, R. J. Cava, and N. P. Ong, Phys. Rev. Lett. **92**, 247001 (2004).
[8] M. Z. Hasan, Y. D. Chuang, D. Qian, Y. W. Li, Y. Kong, A. Kuprin, A. V. Fedorov, R. Kimmerling, E. Rotenberg, K. Rossnagel, Z. Hussain, H. Koh, N. S. Rogado, M. L. Foo, and R. J. Cava, Phys. Rev. Lett. **92**, 246402 (2004).
[9] B. Bernu, P. Lecheminant, C. Lhuillier, and L. Pierre, Phys. Rev. B **50**, 10048 (1994).
[10] Y. Nagaoka, Phys. Rev. **147**, 392 (1966).
[11] J. O. Haerter, M. R. Peterson, and B. S. Shastry, cond-mat/0607293 (unpublished).
[12] B. Kumar and B. S. Shastry, Phys. Rev. B **68**, 104508 (2003).
[13] Y. Hatsugai and M. Kohmoto, Phys. Rev. B **42**, 8282 (1990).
[14] In numerical results with g.s. degeneracies this behavior is somewhat obscured, this is a finite-size effect.
[15] Y. Ishida, H. Ohta, A. Fujimori, and H. Hosono, cond-mat/0511149 (unpublished).
[16] T. Koretsune and M. Ogata, Phys. Rev. Lett. **89**, 116401 (2002).
[17] J. Jaklic and P. Prelovsek, Phys. Rev. Lett. **77**, 892 (1996).
[18] J. Jaklic and P. Prelovsek, Adv. Phys. **49**, 18 (2000).
[19] T. Motohashi, R. Ueda, E. Naujalis, T. Tojo, I. Terasaki, T. Atake, M. Karppinen, and H. Yamauchi, Phys. Rev. B **67**, 064406 (2003).
[20] This discussion expands and supplements the results in Ref. 11 obtained by the same authors.
[21] L. Viciu, J. W. G. Bos, H. W. Zandbergen, Q. Huang, M. L. Foo, S. Ishiwata, A. P. Ramirez, M. Lee, N. P. Ong, and R. J. Cava, Phys. Rev. B **73**, 174104 (2006).
[22] J. L. Gavilano, D. Rau, B. Pedrini, J. Hinderer, H. R. Ott, S. M. Kazakov, and J. Karpinski, Phys. Rev. B **69**, 100404(R) (2004).
[23] B. C. Sales, R. Jin, K. A. Affholter, P. Khalifah, G. M. Veith, and D. Mandrus, Phys. Rev. B **70**, 174419 (2004).
[24] T. Takeuchi, M. Matoba, T. Aharen, and M. Itoh, Physica B **312-313**, 719 (2002).
[25] J. Sugiyama, J. H. Brewer, E. J. Ansaldo, B. Hitti, M. Mikami, Y. Mori, and T. Sasaki, Phys. Rev. B **69**, 214423 (2004).
[26] Y. Ando, N. Miyamoto, K. Segawa, T. Kawata, and I. Terasaki, Phys. Rev. B **60**, 10580 (1999).
[27] H. E. Castillo and C. A. Balseiro, Phys. Rev. Lett. **68**, 121 (1992).
[28] P. Prelovsek, M. Long, T. Markez, and X. Zotos, Phys. Rev. Lett. **83**, 2785 (1999).
[29] P. Prelovsek and X. Zotos, Phys. Rev. B **64**, 235114 (2001).
[30] D. Veberic and P. Prelovsek, Phys. Rev. B **66**, 020408(R) (2002).
[31] X. Zotos, F. Naef, M. Long, and P. Prelovsek, Phys. Rev. Lett. **85**, 377 (2000).
[32] E. Lange, Phys. Rev. B **55**, 3907 (1997).

[33] A. G. Rojo, G. Kotliar, and G. S. Canright, Phys. Rev. B **47**, 9140 (1993).
[34] F. F. Assaad and M. Imada, Phys. Rev. Lett. **74**, 3868 (1995).
[35] P. N. Mahesh and B. S. Shastry, Physica B **223-224**, 501 (1996).
[36] N. P. Ong, Phys. Rev. B **43**, 193 (1991).
[37] O. I. Motrunich and P. A. Lee, Phys. Rev. B **69**, 214516 (2004).
[38] P. W. Anderson, Phys. Rev. Lett. **67**, 2092 (1991).
[39] T. D. Stanescu and P. Phillips, Phys. Rev. B **69**, 245104 (2004).
[40] M. Grayson, L. B. Rigal, D. C. Schmadel, H. D. Drew, and P. J. Kung, Phys. Rev. Lett. **89**, 037003 (2002).
[41] B. S. Shastry and B. Sutherland, Phys. Rev. Lett. **65**, 243 (1990).